Pergamon

Int. J. Heat Mass Transfer. Vol. 41, Nos 8–9, pp. 1113–1125, 1998
© 1997 Elsevier Science Ltd. All rights reserved
Printed in Great Britain
0017-9310/98 $19.00+0.00

PII: S0017-9310(97)00155-5

Transient natural convection in a vertical cylinder opened at the extremities and filled with a fluid saturated porous medium: validity of Darcy flow model and thermal boundary layer approximations

K. SLIMI and S. BEN NASRALLAH

Laboratoire des Transferts de Chaleur et de Masse, Ecole Nationale d'Ingénieurs de Monastir, Route de Kairouan, 5019 Monastir, Tunisie

and

J.-P. FOHR

Laboratoire d'Etudes Thermiques (UA CNRS 1403), 40, Avenue du Recteur Pineau, 86022 Poitiers, France

(*Received* 6 *December* 1996 *and in final form* 20 *March* 1997)

Abstract—The purpose of the present paper is to analyse numerically the flow and heat transfer by transient natural convection in a vertical cylinder filled with a fluid saturated porous medium. The cylinder is opened at both ends and heated with a constant wall heat flux density. This study is carried out using the Forchheimer-extended Darcy flow model and a two-temperature model. The velocity, temperature and pressure drop distributions, the dimensionless flow rate q_v^* and heat flux exchanged at the cylinder exit Φ^* are obtained under various conditions. The results presented in this work provide also the validity of Darcy flow model and thermal boundary layer approximations. © 1997 Elsevier Science Ltd.

1. INTRODUCTION

Since the early work of Darcy, extensive investigations have been conducted on flow and heat transfer in porous media. The need of fundamental studies on fluid flow and heat transfer in saturated porous media stems from the fact that a better understanding of a host of engineering applications in which porous materials are present is required. Examples of engineering applications which stand to benefit from a better understanding of fluid flow and heat transfer processes through porous materials are: geothermal reservoir engineering, oil extraction, thermal insulation, packed bed chemical reactors, grain storage, oil extraction, the manufacturing of numerous products in the chemical industry, adsorption and desorption applications, etc.

Natural convection in porous medium has been studied by many investigators. Among the published works, we find those related to the stability problems. An exhaustive review of the published work related to this problem is presented in the papers of Bories [1], Combarnous and Bories [2], Cheng [3] and Nield [4].

The problem of a heat source embedded in a porous medium has been the subject of many studies [5–9]. Natural convection flow and heat transfer over a flat plate in porous medium are available in the literature [10–14]. The problem of natural convection in confined geometry has been treated by an increasing number of investigators. Among the investigations related to this problem, we find those of Bejan [15], Weber [16], Mazuouka *et al.* [17], Beukema [18], Ineba and Sekin [19], Lauriat and Prasad [20], Chang and Hsiao [21] and Combarnous and Bories [22].

Natural convection in semi-confined porous medium studies are few in the available literature. Among the related reviews about natural convection in semi-confined geometry, we find the work of Bejan [23], and Thibaud [24], which considered a vertical cylinder opened at the extremities with a stationary natural heat convection caused by a lateral uniform heat flux density, Young *et al.* [25], which considered a cavity opened at its top extremity and presented a liner heat source in the interior, and Nishimura *et al.* [26] on flow and heat transfer in a cavity partially filled with a porous medium and heated differentially at its lateral walls. Recently, Ben Nasrallah *et al.* [27] conducted a numerical study of unsteady natural convection in the same geometrical configuration of a silo (cylindrical,

NOMENCLATURE

A	aspect ratio of the cylinder, R/H
a_{fs}	solid–fluid exchange area [m^2]
Bi^*	modified Biot number representing the internal change, $h_{fs}H^2a_{fs}/k_f$
Bi	Biot number representing the change between the outlet face of the cylinder and the ambient, hH/k_f
c_{pf}	specific heat capacity of the fluid at constant pressure [J kg^{-1} K^{-1}]
c_{ps}	specific heat capacity of the solid at constant pressure [J kg^{-1} K^{-1}]
Da	Darcy number, k/H^2
d_p	average particle diameter [m]
F	Forchheimer number
g	acceleration due to gravity [m s^{-2}]
Gr_f	fluid Grashof number, $g\beta qH^4/v_f^2k_f$
H	cylinder height [m]
h	heat transfer coefficient at the cylinder exit [W m^{-2} K^{-1}]
h_{fs}	particle-to-fluid heat transfer coefficient [W m^{-2} K^{-1}]
k	permeability of the porous medium [m^2]
k_f	thermal conductivity of the fluid [W m^{-1} K^{-1}]
k_s	thermal conductivity of the solid [W m^{-1} K^{-1}]
P	motorise pressure [N m^{-2}]
P_0	ambient pressure [N m^{-2}]
Pr_f	fluid Prandtl number, v_f/α_f
q	heat flux density [W m^{-2}]
q_v	flow rate [m^3 s^{-1}]
r	radial coordinate [m]
R	cylinder radius [m]
Re	Reynolds number based on the inlet velocity and the cylinder height, ρ_fU_0H/μ_f
Re_d	Reynolds number based on the velocity scale and the particle diameter, $\rho_fU_{ref}d_p/\mu_f$
TBLA	thermal boundary layer approximations
t	time [s]
T_0	ambient temperature [K]
T_f, T_s	temperature of the fluid and the solid, respectively [K]
u, v	axial and transverse velocity components [m s^{-1}]
U, V	dimensionless axial and transverse velocity components
$\mathbf{V}$	velocity vector [m s^{-1}]
$\boldsymbol{V}$	dimensionless velocity vector
X	dimensionless transverse coordinate
z	axial coordinate [m]
Z	dimensionless axial coordinate.

Greek symbols

α_f	thermal diffusivity of the fluid, $\alpha_f = k_f/(\rho c_p)_f$ [m^2 s^{-1}]
α_s	thermal diffusivity of the solid, $\alpha_s = k_s/(\rho c_p)_s$ [m^2 s^{-1}]
β	fluid coefficient of volume expansion [K^{-1}]
ε	average porosity of the porous medium
θ_f, θ_s	dimensionless temperature of the fluid and the solid, respectively
Λ_H	inertia parameter, $\varepsilon FH/\sqrt{k}$
μ_f	fluid's dynamic viscosity [kg (ms)$^{-1}$]
v_f	fluid's kinematic viscosity [m^2 s^{-1}]
Π	dimensionless pressure
ρ_f	fluid's density [kg m^{-3}]
ρ_s	solid's density [kg m^{-3}]
τ	dimensionless time
Φ	heat flux exchanged at the cylinder exit [W].

Subscripts

f	fluid phase
s	solid phase
ref	reference
D	Darcy flow model
(n,m)	space indexes
i	time index.

Superscript

*	dimensionless quantity.

open extremities). The authors have used the Darcy flow model and assumed that the effective thermal conductivity of the fluid phase as well as the fluid-to-solid heat transfer coefficient are constant. As far as we know, we can conclude that:

- To the author's knowledge, the problem of unsteady two-dimensional natural convection in a vertical cylinder opened at the extremities and filled with a fluid-saturated porous medium that determine the validity domains of the thermal boundary layer approximations and of the Darcy flow model, is not studied.
- The sensitivity to fluid Prandtl and Darcy numbers of the flow and heat transfer by natural convection in a vertical cylinder filled with a porous medium opened at its both extremities and heated with a uniform lateral heat flux is not studied. Ben Nasrallah *et al.* [27] have studied only the effect of the fluid Grashof number.

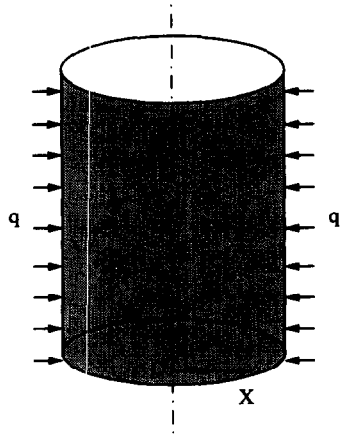

Fig. 1. Geometrical configuration.

In the present paper, we aim to study the problem of unsteady natural convection which occurs in a vertical cylinder opened at both ends, filled with a fluid-saturated porous medium and heated with a uniform lateral heat flux density. The present study is carried out using the Forchheimer-extended Darcy flow model, which accounts for both inertia and thermal dispersion effects. A two-temperature model is used for energy transport. The set of equations is resolved by the finite volume method [28]. A comparison between results obtained with the widely-used Darcy flow model and the Forchheimer-extended Darcy model demonstrates the importance of inertial effects in porous media. The description of the physical phenomena, the dependence of the temperature and flow fields on the flow and heat transfer governed parameters, as well as the validity domains of the Darcy flow model and thermal boundary layer approximations (TBLA), are also reported in the course of this study.

2. MATHEMATICAL FORMULATION

A schematic of the physical model and coordinate system is shown in Fig. 1. It is assumed that the flow in the cylinder is two-dimensional. The porous medium is considered to be homogeneous, isotropic and is saturated with a pure single phase fluid, which is not in thermal equilibrium with the solid matrix. The thermophysical properties of the solid matrix and the fluid are assumed to be constant, except in the body force term of the momentum equations invoking the Boussinesq's approximation. Although the porosity vary near the wall [29], the current study assumes constant porosity throughout the cylinder and the validity of the Darcy–Forchheimer flow model without transient term.

The analysis is made in terms of non-dimensional parameters that successfully cast together all the pertinent influencing effects. To this end, the non-dimensionalization of the governing equations at a macroscopic scale, is carried out on the basis of the following definitions:

$$L_{\mathrm{ref}} = H, \quad \Delta T_{\mathrm{ref}} = \frac{qH}{k_{\mathrm{f}}}, \quad P_{\mathrm{ref}} = \frac{k_{\mathrm{f}}}{(\rho c_{\mathrm{p}})_{\mathrm{f}}}\frac{\mu_{\mathrm{f}}}{k},$$

$$U_{\mathrm{ref}} = \frac{k}{\mu_{\mathrm{f}}}\frac{P_{\mathrm{ref}}}{H}, \quad t_{\mathrm{ref}} = \frac{H}{U_{\mathrm{ref}}} \tag{1}$$

where the nondimensional quantities are

$$X = \frac{r}{H}, \quad Z = \frac{z}{H}, \quad \theta_{\mathrm{f}} = \frac{T_{\mathrm{f}} - T_0}{\Delta T_{\mathrm{ref}}},$$

$$\theta_{\mathrm{s}} = \frac{T_{\mathrm{s}} - T_0}{\Delta T_{\mathrm{ref}}}, \quad \Pi = \frac{P - P_0}{P_{\mathrm{ref}}},$$

$$U = \frac{u}{U_{\mathrm{ref}}}, \quad V = \frac{v}{U_{\mathrm{ref}}}, \quad \tau = \frac{t}{t_{\mathrm{ref}}}. \tag{2}$$

The resulting continuity, momentum and energy equations in terms of dimensionless variables are as follows:

Continuity

$$\nabla \cdot \boldsymbol{V} = 0. \tag{3}$$

Momentum

$$U = -\frac{\partial \Pi}{\partial Z} + Gr_{\mathrm{f}} \cdot Da \cdot Pr_{\mathrm{f}}\theta_{\mathrm{f}} - \frac{\Lambda_{\mathrm{H}} \cdot Da}{Pr_{\mathrm{f}}}|\boldsymbol{V}|U;$$

$$V = -\frac{\partial \Pi}{\partial X} - \frac{\Lambda_{\mathrm{H}} \cdot Da}{Pr_{\mathrm{f}}}|\boldsymbol{V}|V \tag{4}$$

where $\boldsymbol{V}$ is the dimensionless velocity, Λ_{H} is the inertia parameter defined as $\Lambda_{\mathrm{H}} = \varepsilon FH/\sqrt{k \cdot k}$ is the permeability of the porous media and F is an empirical coefficient which depends upon the permeability as well as the microstructure of the porous matrix which accounts for the inertial effects or second-order flow resistance, due to recirculatory flows inside pore volumes. The value ofthe Forchheimer number F, is related to the form drag caused by the porous matrix. Experimental results conducted by Ward [30] have suggested that F is close to 0.55. However, care should be taken in choosing such a value for F. The values of F and k used in all the calculations executed in this study are determined according to the following relations [31]:

$$k = \frac{\varepsilon^3 d_{\mathrm{p}}^2}{150(1-\varepsilon)^2}, \quad F = \frac{1.75}{\sqrt{150}\varepsilon^{3/2}}. \tag{5}$$

Da is the Darcy number based on the permeability of the porous media and the height H of the cylinder: $Da = k/H^2$, Pr_{f} is the fluid Prandtl number, $Pr_{\mathrm{f}} = \nu_{\mathrm{f}}/\alpha_{\mathrm{f}}$ and Gr_{f} is the fluid Grashof number defined as $Gr_{\mathrm{f}} = g\beta qH^4/\nu_{\mathrm{f}}^2 k_{\mathrm{f}}$.

Fluid phase energy

$$\varepsilon\frac{\partial \theta_{\mathrm{f}}}{\partial \tau} + \boldsymbol{V} \cdot \nabla\theta_{\mathrm{f}} = \left\{\frac{1}{X}\frac{\partial}{\partial X}\left[X(k_{\mathrm{feff}})_X \frac{\partial \theta_{\mathrm{f}}}{\partial X}\right] + \frac{\partial}{\partial Z}\left[(k_{\mathrm{feff}})_Z \frac{\partial \theta_{\mathrm{f}}}{\partial Z}\right]\right\} - Bi^*(\theta_{\mathrm{f}} - \theta_{\mathrm{s}}). \tag{6}$$

$(k_{\text{feff}})_X = \varepsilon + 0.1 Pr_f Re_d V$ and $(k_{\text{feff}})_Z = \varepsilon + 0.5 Pr_f Re_d U$ and $Bi^* = h_{fs} a_{fs} H^2 / k_f$ is the modified Biot number, and a_{fs} is the solid–fluid exchange area which is formulated as [32]:

$$a_{fs} = \frac{6(1-\varepsilon)}{d_p}. \tag{7}$$

The formulation of the fluid-to-solid heat transfer coefficient in the present investigation was based on an empirical correlation stated by Wakao *et al.* [33]:

$$h_{fs} = \frac{k_f}{d_p}\left[2 + 1.1 Pr_f^{1/3}\left(\frac{\rho_f u d_p}{\mu_f}\right)^{0.6}\right]. \tag{8}$$

In the present study, the dispersion phenomenon is dealt with as an additional diffusive term added to the stagnant component [34]. The stagnant component is expressed in terms of the individual thermal conductivities of the phases and the phase porosities. To model the effective conductivities, we have resorted to the empirical correlation developed by Wakao and Kaguei [36] as follows:

$$(k_{\text{feff}})_r = \varepsilon k_f + 0.1\left[Pr_f\left(\frac{\rho_f u d_p}{\mu_f}\right)\right]k_f$$

$$(k_{\text{feff}})_z = \varepsilon k_f + 0.5\left[Pr_f\left(\frac{\rho_f u d_p}{\mu_f}\right)\right]k_f \tag{9}$$

$$(k_{\text{seff}}) = (1-\varepsilon)k_s. \tag{10}$$

Solid phase energy

$$(1-\varepsilon)\frac{\partial \theta_s}{\partial \tau} = \frac{\alpha_s}{\alpha_f}\left\{(1-\varepsilon)\left[\frac{1}{X}\frac{\partial}{\partial X}\left(X\frac{\partial \theta_s}{\partial X}\right) + \frac{\partial}{\partial Z}\left(\frac{\partial \theta_s}{\partial Z}\right)\right] + \frac{k_f}{k_s} Bi^*(\theta_f - \theta_s)\right\}. \tag{11}$$

Because the buoyancy effects are significant in the region close to the wall, due to the applied heat flux density, the temperature and velocity gradients are important in that region. Indeed, the thickness of the boundary layer on the cylindrical wall increases with the height and the decrease of the wall heat flux. So, in the present investigation, emphasis will be placed on the validity domain of thermal boundary layer approximations, which are extensively used by an increasing number of investigators. Assuming that the thermal boundary layer approximations are applicable, the second-order derivatives in the Z-direction of the temperature field are negligible compared to those in the X-direction. In a non-dimensional form, the relevant initial, boundary hydrodynamic and thermal conditions are written as follows.

2.1. *Initial and boundary hydrodynamic conditions*

Initially (at $\tau \leqslant 0$), we assume that the motorise pressure in the cylinder is uniform and equal to the ambient pressure. This is represented by equation (12).

$$\Pi(X, Z, 0) = 0. \tag{12}$$

The fluid gets into the cylinder and out of it at the same pressure. Accordingly, at $Z = 0$ and 1, for $0 < X < A$:

$$\Pi(X, 0, \tau) = \Pi(X, 1, \tau) = 0 \tag{13}$$

where A is the cylinder ratio, $A = R/H$. Owing to the symmetry requirement at the cylinder centreline (at $X = 0$, for $0 < Z < 1$), it follows that:

$$\frac{\partial \Pi}{\partial X}(0, Z, \tau) = 0. \tag{14}$$

The lateral surface of the cylinder is impermeable. This is interpreted by:

$$\frac{\partial \Pi}{\partial X}(A, Z, \tau) = 0. \tag{15}$$

2.2. *Initial and boundary thermal conditions*

Initially, the fluid and the solid are assumed to be at the same temperature:

$$\theta_f(X, Z, 0) = \theta_s(X, Z, 0) = 0. \tag{16}$$

The fluid enters the cylinder at constant temperature:

$$\theta_f(X, 0, \tau) = 0. \tag{17}$$

The heat transfer between the solid particles and the surrounding fluid are modelled by a heat transfer coefficient:

$$(1-\varepsilon)\frac{\partial \theta_s}{\partial Z}(X, 0, \tau) = Bi^* \frac{k_f}{k_s}\theta_s(X, 0, \tau). \tag{18}$$

Owing to the symmetry requirement at the cylinder centreline (at $X = 0$, for $0 < Z < 1$), it follows that:

$$\frac{\partial \theta_f}{\partial X}(0, Z, \tau) = \frac{\partial \theta_s}{\partial X}(0, Z, \tau) = 0. \tag{19}$$

Constant wall heat flux is applied at the lateral surface. This is expressed by the following boundary condition [35]:

$$(k_{\text{feff}})_X \frac{\partial \theta_f}{\partial X}(A, Z, \tau) = 1, \quad (1-\varepsilon)\frac{\partial \theta_s}{\partial X}(A, Z, \tau) = \frac{k_f}{k_s}. \tag{20}$$

At the cylinder exit, the existent flow in the upper porous surface is very complicated. On one hand the upper face releases a natural convection fluid flow similar to that observed over a heated horizontal flat plate. On the other hand the outlet fluid flow disturbs the effect of the heated horizontal flat plate and, under certain conditions, it can allow fluid to re-enter the cylinder as a recirculatory flow. To rigorously solve this problem, we are expected to make the calculating

domain larger in order to take into account the fluid flow and heat transfer near the outlet face, which will complicate the study. To avoid this problem we introduce, in the case of an upward flow ($U > 0$), a heat transfer coefficient as follows:

$$-\frac{\partial\theta_f}{\partial Z}(X,1,\tau) = Bi\theta_f(X,1,\tau). \quad (21a)$$

In the case of a downward flow ($U < 0$), the boundary condition for the fluid phase at the cylinder exit is:

$$\theta_f(X,1,\tau) = 0. \quad (21b)$$

At the cylinder exit, we use for the solid phase the following boundary condition:

$$(1-\varepsilon)\frac{\partial\theta_s}{\partial Z}(X,1,\tau) = Bi^*\frac{k_f}{k_s}\theta_s(X,1,\tau). \quad (21c)$$

3. NUMERICAL RESOLUTION

The governing equations with the associated boundary conditions are solved by the finite volume method initiated by Patankar [13], which is based on the solution of difference equations obtained by integrating the differential equations for momentum and energy over control volume enclosing the nodal points.

To examine the validity of our numerical scheme, the numerical results were compared with the most closely related numerical solutions. This was achieved by making the necessary adjustments to our model to reduce it to a system equivalent to the simplified available cases. Our numerical results for the velocity and temperature distributions were compared with the numerical results obtained by Ben Nasrallah *et al.* [27] by making the necessary changes (we put $Da \to 0$, $k_{feff} = \varepsilon k_f$, $k_{seff} = (1-\varepsilon)k_s$ and h_{fs} is considered as a constant). They all agree at least up to three decimal places. The comparison is not shown here for the sake of brevity.

We have presented, for different parameters (Gr_f, Pr_f, Da, $\Lambda_H \ldots$), the time–space evolution of the temperature, pressure and velocity. We have also presented the dimensionless flow rate, q_v^*, and heat flux, Φ^*, exchanged at the cylinder exit. These two variables are obtained with integration over the whole section and at the cylinder exit (i.e. at $Z = 1$), and are written in a dimensionless form based on the following definitions:

$$q_{vref} = \pi R^2 U_{ref} \quad \text{and} \quad \Phi_{ref} = 2\pi RHq. \quad (22)$$

In a dimensionless form, these two variables are written as follows:

$$q_v^* = \frac{2}{A^2}\int_0^A UX\,dX,$$

$$\Phi^* = \frac{1}{A}\left[\int_0^A U\theta_f X\,dX + Bi\int_0^A \theta_f X\,dX + \frac{Bi^*}{H\cdot a_{fs}}\int_0^A \theta_s X\,dX\right]. \quad (23)$$

We have chosen these two variables because, on one hand their representations are of great interest, especially for many industrial applications where it is necessary to have an idea on the amount of heat that can be recaptured at the exit of the silo and/or the flow rate. On the other hand, they allow us to distinguish easily the effect of different parameters and the validity domains of different assumptions (i.e. Darcy flow model and TBLA).

3.1. *Description of the phenomena*

The results of numerical simulation are presented as isovalue curves giving the time–space evolution of the temperature, pressure and velocity. In this section, all the calculations have been performed for a Biot number representing the external change (between the porous medium and the ambient), $Bi = 2\times10^3$ and an inertia coefficient $\Lambda_H = 0.057$. A typical value of the porosity of a randomly-packed sphere of 1 mm diameter, $\varepsilon = 0.4$, is used for the numerical solutions reported here. This fixes the value of F in equation (5) as 0.56. The numerical simulation was carried out for different values of the Grashof number, Gr_f and aspect ratio of the cylinder, A. The numerical results show two classes of flows (with and without top aspiration) which depend upon the values of Gr_f, Da, Pr_f and A.

3.1.1. *Flow with top aspiration.* The flow with top aspiration is found for high aspect ratio, A or great values of fluid Grashof number and/or Darcy number. Flow with top aspiration is also found for higher values of fluid Prandtl number. For a given value of Darcy number, $Da = 10^{-2}$ and a fluid Prandtl number, $Pr_f = 0.71$, typical values of fluid Grashof number and aspect ratio ($Gr_f = 2\times10^8$ and $A = 1$) have been chosen to illustrate such a type of flow. Figure 2(a) shows that the renewal air induced by the wall heating is partially aspired from the top and partially from the base of the cylinder. This is due to the bulk frictional drag induced by the solid matrix. So, the fluid re-enters the cylinder as a recirculatory flow represented by negative values of the centreline axial velocity. Figure 2(a) shows also that the axial velocity decreases near the axis, attains a negative minimum and then increases. Near the wall region [Fig. 2(b)], the axial velocity increases due to the buoyancy effects, reaches a positive maximum and then decreases due to the presence of the motorise ambient pressure which decelerates the flow.

Figure 3 depicts the time-space variations of pressure within the cylinder. As can be seen, the pressure decreases from the inlet, attains a minimum value and increases, attains a maximum and decreases to reach the ambient pressure. The pressure decreases at first

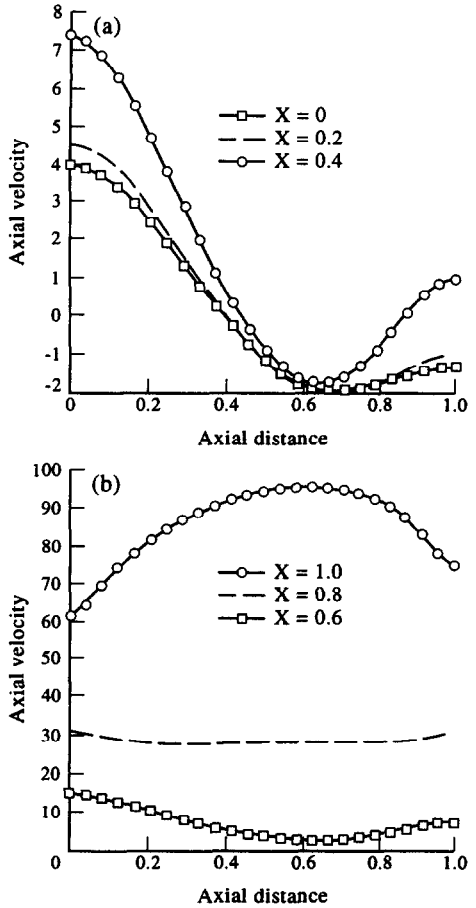

Fig. 2. Axial velocity vs axial distance for $Gr_f = 2 \times 10^8$, $A = 1$, $Pr_f = 0.71$, $Da = 10^{-2}$, $\alpha_f/\alpha_s = 0.16$, $Bi = 2 \times 10^3$ and $\Lambda_H = 0.057$. (a) $0 \leqslant X \leqslant 0.4$ and (b) $X > 0.4$.

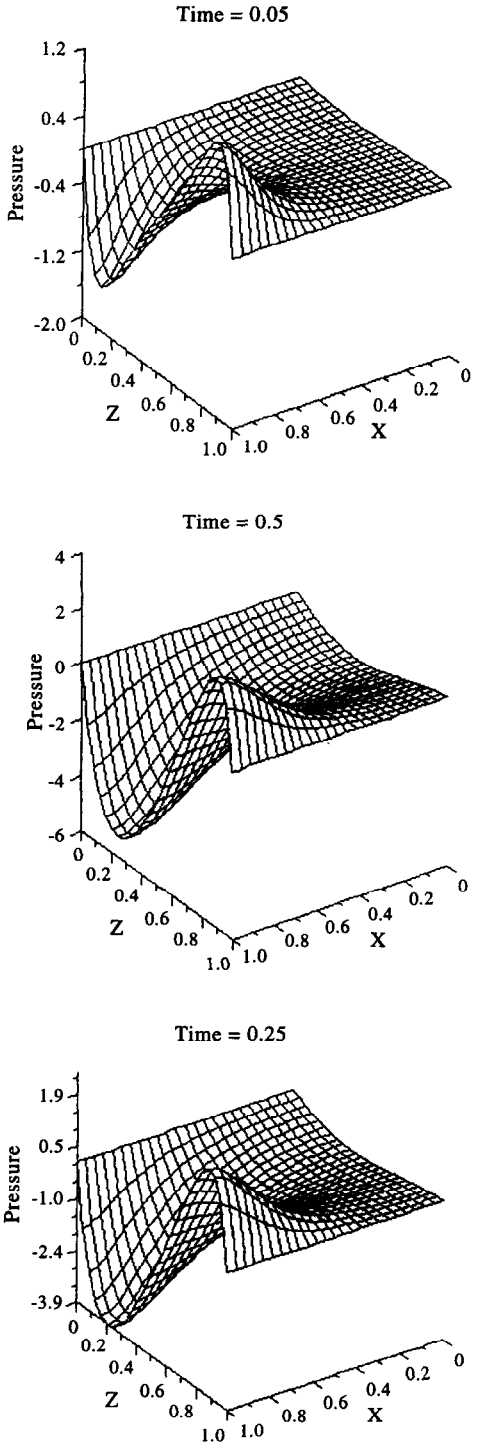

Fig. 3. Time–space variations of pressure for $Gr_f = 2 \times 10^8$, $A = 1$, $Pr_f = 0.71$, $Da = 10^{-2}$, $\alpha_f/\alpha_s = 0.16$, $Bi = 2 \times 10^3$ and $\Lambda_H = 0.057$.

with time and, for enough period of time, it tends to be independent of time (steady-state regime). As is illustrated in Fig. 4, the z-component of the velocity is important in a region close to the heated wall and decreases with the radial distance, X.

Figure 5 indicates the time–space variations of the fluid phase temperature within the cylinder. The isotherms have the same profile found in the case of a heated flat plate in a semi-infinite medium and are confined in the region near the heated boundary. Due to the applied lateral heat flux density, the fluid phase temperature is found to be important in a region close to the heated wall. At the cylinder exit, the vertical fluid phase temperature gradients are high because of the heat loss to surroundings. However, the influencing region of these thermal gradients is very scanty.

3.1.2. *Chimney-type flow.* A convective flux of a chimney type is found for small aspect ratio, A or small values of fluid Grashof number and/or lower Prandtl and Darcy numbers. For a given Darcy number, $Da = 10^{-2}$ and a fluid Prandtl number, $Pr_f = 0.71$, typical values of fluid Grashof number and aspect ratio ($Gr_f = 10^8$ and $A = 0.1$) have been chosen to illustrate such a type of flow.

The velocity component in the transverse direction is approximately equal to zero, since the isobars are near the horizontal (Fig. 6). As expected, the axial velocity is important near the heated wall and increases in the axial direction due to the buoyancy

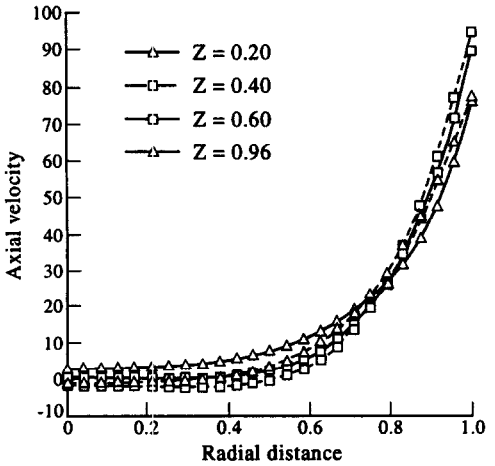

Fig. 4. Axial velocity vs radial distance for $Gr_f = 2 \times 10^8$, $A = 1$, $Pr_f = 0.71$, $Da = 10^{-2}$, $Bi = 2 \times 10^3$, $Z = 1$, $\alpha_f/\alpha_s = 0.16$ and $\Lambda_H = 0.057$.

effects as can be observed in Fig. 7. Near the outlet face of the cylinder, the axial velocity decreases. This decrease of the axial velocity values is due to the presence of the ambient motorise pressure.

As shown in Fig. 8, the radial temperature gradients are very low. The axial temperature gradients are very important near the exit of the cylinder as was explained previously and they occupied the whole exit area.

3.2. *Sensitivity to the parameters*

We have studied the effect of the Darcy number, Da, and fluid Prandtl number, Pr_f, on fluid flow and heat transfer in the cylinder. The computations have been carried out for an aspect ratio, $A = 0.5$, a Biot number, $Bi = 2 \times 10^3$ and for different fluid Grashof number ranging from 10^8 to 5×10^9. To understand properly the effect of the porous matrix scaling, Da, we have presented, in Fig. 9, the fluid phase temperature and the velocity fields for $Da = 10^{-6}$–10^{-2}.

Figure 9(a) and (b) shows the change in the centre-

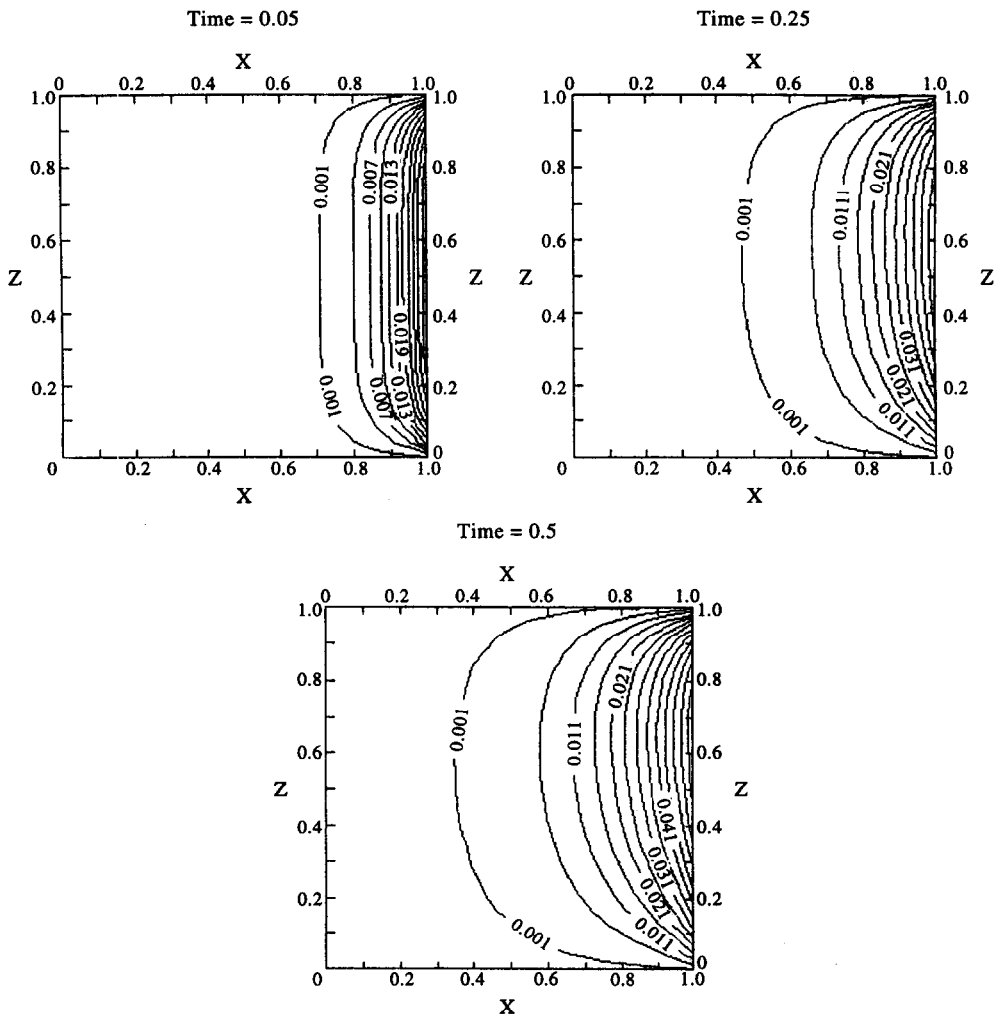

Fig. 5. Time–space variations of fluid phase temperature for $Gr_f = 2 \times 10^8$, $A = 1$, $Pr_f = 0.71$, $Da = 10^{-2}$, $Bi = 2 \times 10^3$, $\alpha_f/\alpha_s = 0.16$ and $\Lambda_H = 0.057$.

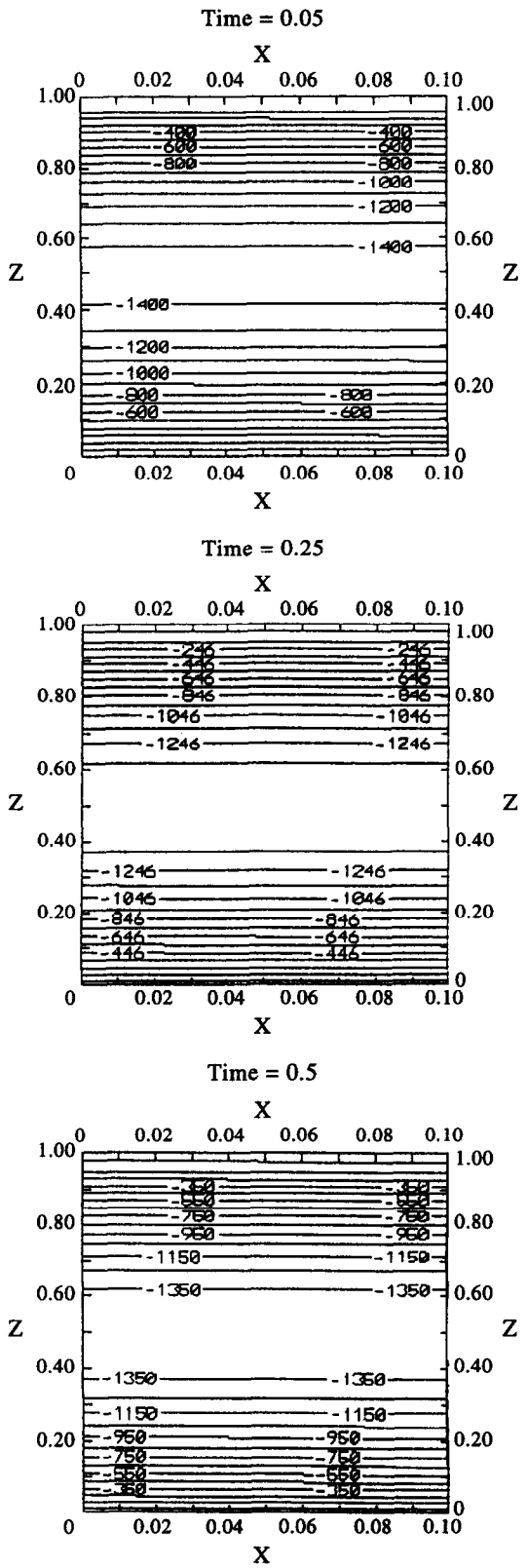

Fig. 6. Time–space variations of pressure for $Gr_f = 10^8$, $A = 0.1$, $Pr_f = 0.71$, $Da = 10^{-2}$, $Bi = 2 \times 10^3$, $\alpha_f/\alpha_s = 0.16$ and $\Lambda_H = 0.057$.

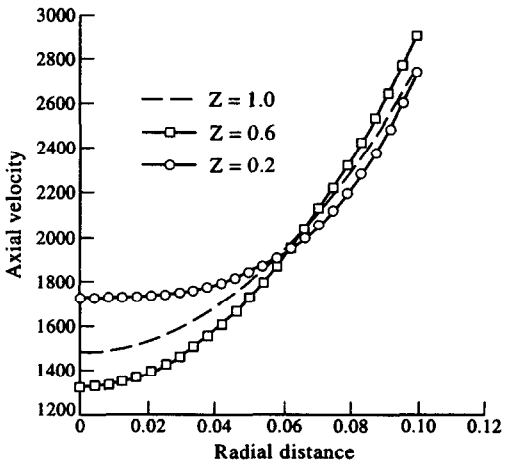

Fig. 7. Axial velocity vs radial distance for $Gr_f = 10^8$, $A = 0.1$, $Pr_f = 0.71$, $Da = 10^{-2}$, $\Lambda_H = 0.057$, $\alpha_f/\alpha_s = 0.16$, $Bi = 2 \times 10^3$ and at different axial distance.

line axial velocity and fluid phase temperature vs axial distance for representative values of Darcy number ranging from 10^{-6} (i.e. for a densely-packed medium) to 10^{-2} (i.e. larger particle size). As has been seen, aspiration is increased with the Darcy number leading to a decrease in the fluid temperature. This is evident, because for a given system, the flow intensity and thermal activity increase with the Darcy number since the permeability of the porous matrix has increased, thereby reducing the resistance to flow. Figure 9(b) shows also that the maximum of the fluid phase temperature moves towards to the exit as the Darcy number increases from 10^{-6} to 10^{-2}. These thermal and flow fields behaviours are similar for all fluid Grashof numbers used in this study.

The influence of the porous medium inertia coefficient Λ_H effects on the flow and heat transfer parameters is the same as that of the inverse Darcy number since it also represents resistance to flow. Therefore, as Λ_H increases, the axial velocity, U, decreases while the fluid phase temperature, θ_f, increases, respectively. To examine the effects of fluid Prandtl number Pr_f, the numerical solutions were obtained for $Pr_f = 1$ to 10^2, for $Gr_f = 2 \times 10^8$ and with $Da = 10^{-4}$. These values of Pr_f were selected in order to represent, low, moderate and high Prandtl number regimes.

The centreline axial velocity and fluid phase temperature profiles for $Pr_f = 1$, 10 and 100 are presented in Fig. 10(a) and (b). These plots indicate that the absolute values of the flow velocity increase with the fluid Prandtl number. With an increase in the fluid Prandtl number, the recirculatory flow intensifies [see Fig. 10(a)]. Figure 10(b) shows that the fluid phase temperature decreases with an increase of the fluid Prandtl number and the maximum of the fluid phase temperature moves towards the outlet of the cylinder as the Prandtl number increases.

Significant changes in the velocity and fluid temperature fields with Pr_f are further shown in Fig. 11(a)

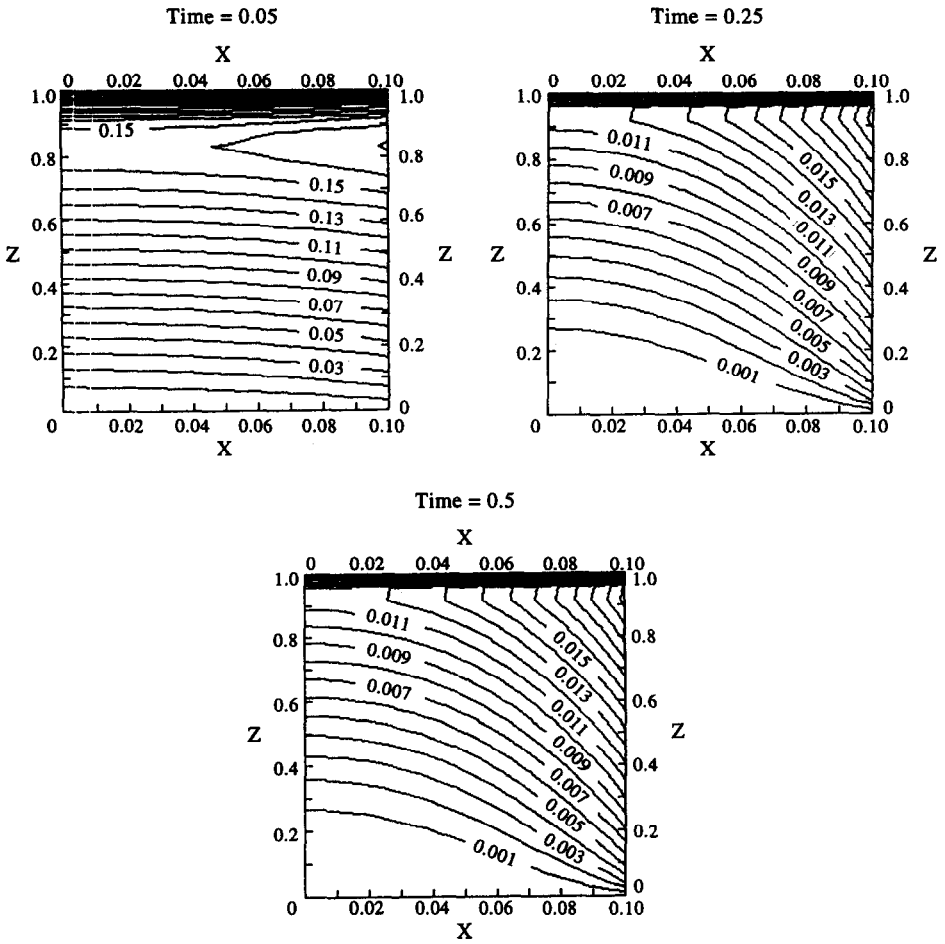

Fig. 8. Time–space variations of fluid phase temperature for $Gr_f = 10^8$, $A = 0.1$, $Pr_f = 0.71$, $\alpha_f/\alpha_s = 0.16$, $Da = 10^{-2}$, $Bi = 2 \times 10^3$ and $\Lambda_H = 0.057$.

and (b), where the vertical velocity and the fluid phase temperature profiles at the midheight (i.e. at $Z = 0.5$) and the mid-plane (i.e. at $X = 0.25$) are presented for $Pr_f = 1$, 10, 100. Near the wall, the velocity increases substantially with an increase in the Prandtl number. However, the effect may be reversed away from the heated wall [Fig. 11(a)]. The increase in the flow field with Prandtl number leads to a decrease in the thermal field [Fig. 11(b)].

3.3. *Validity of the Darcy flow model*

The examination of the validity of the Darcy flow model was carried out by comparing the values of the flow rate and the heat flux exchanged at the cylinder exit obtained by the Darcy flow model and the Darcy–Forchheimer model. This may be expressed in the following form:

$$\%\Phi^* = \left|1 - \frac{\Phi_D^*}{\Phi^*}\right| \times 100 \quad \text{and} \quad \%q_v^* = \left|1 - \frac{q_{v_D}^*}{q_v^*}\right| \times 100 \tag{24}$$

where $q_{v_D}^*$ and Φ_D^* are, respectively, the dimensionless flow rate and the dimensionless heat flux exchanged at the cylinder exit obtained with the Darcy flow model.

From the following table we can conclude that the Darcy flow model becomes less pronounced in the steady state regime as Da and Gr_f increase or Λ_H and Pr_f decrease. This is obvious because, for greater values of Darcy and fluid Grashof numbers or lower values of the inertia parameter and fluid Prandtl numbers, the flow intensity becomes stronger leading to an increase in the velocity fields and then the applicability of the Darcy flow model becomes questionable. If $Da \leqslant 10^{-4}$, the Darcy flow model is a very good one for all fluid Grashof numbers ranging from 10^8 to 5×10^9 and for all fluid Prandtl numbers ranging from 1 to 100.

3.4. *Validity of the thermal boundary layer approximations (TBLA)*

In order to test the validity of TBLA, the computations have been carried out for various value of

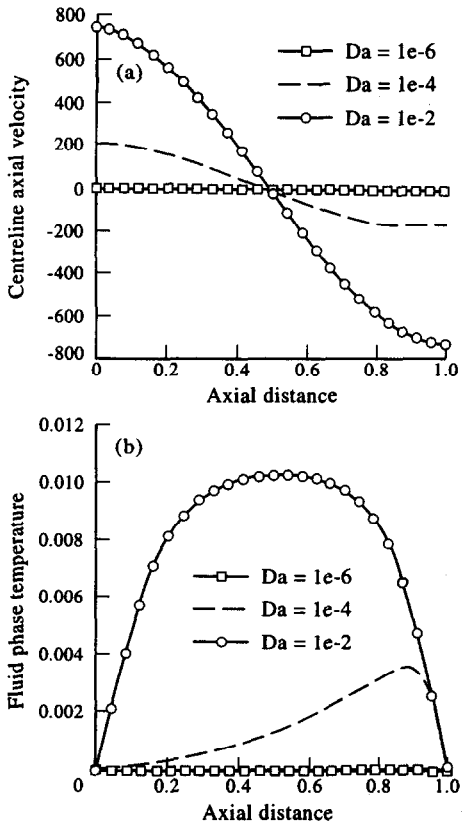

Fig. 9(a) Centreline axial velocity; and (b) fluid phase temperature variations with axial distance for $Gr_f = 10^9$, $A = 0.5$, $Pr_f = 0.71$, $\Lambda_H = 0.057$, $\alpha_f/\alpha_s = 0.16$, $X = 0.5$, $Bi = 2 \times 10^3$ and for representative values of Darcy number.

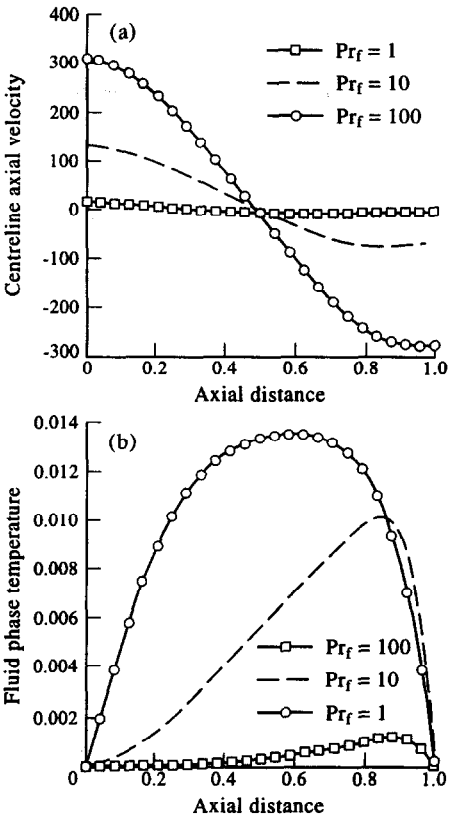

Fig. 10(a) Centreline axial velocity vs axial distance; (b) fluid phase temperature variations with axial distance at $X = 0.5$ and for $Gr_f = 10^8$, $A = 0.5$, $Da = 10^{-4}$, $\alpha_f/\alpha_s = 0.16$, $\Lambda_H = 0.057$, $Bi = 2 \times 10^3$ and for representative values of Prandtl number.

Gr_f	$Pr_f = 0.71$ $\%\Phi^*$	$Da = 10^{-6}$ $\%q_v^*$	$Pr_f = 0.71$ $\%\Phi^*$	$Da = 10^{-4}$ $\%q_v^*$	$Pr_f = 0.71$ $\%\Phi^*$	$Da = 10^{-2}$ $\%q_v^*$
10^8	6.75×10^{-3}	6.37×10^{-5}	1.67	1.87×10^{-1}	4.53	52.72
10^9	7.72×10^{-2}	3.89×10^{-4}	1.78	7.20×10^{-1}	13.12	67.93
5×10^9	3.32×10^{-1}	1.18×10^{-3}	1.98	1.64	13.38	75.23
Pr_f	$Gr_f = 10^8$	$Da = 10^{-6}$	$Gr_f = 10^8$	$Da = 10^{-4}$	$Gr_f = 10^8$	$Da = 10^{-2}$
1	3.20×10^{-2}	2.40×10^{-2}	7.50×10^{-3}	1.62×10^{-1}	5.78	50.50
10	2.31×10^{-6}	3.71×10^{-5}	3.79×10^{-3}	6.58×10^{-2}	5.01	34.58
100	0.62×10^{-6}	2.87×10^{-5}	1.46×10^{-3}	2.59×10^{-2}	3.11	19.90

$\%q_v^*$ and $\%\Phi^*$, in the steady state regime, for $A = 0.5$, $\alpha_f/\alpha_s = 0.16$ and $\Lambda_H = 0.057$.

Gr_f, Bi, Pr_f, Da and for an aspect ratio, $A = 0.5$. To this end, we have made two types of comparisons: comparisons of local values of the fluid phase temperature and of velocity distributions obtained with and without TBLA and comparisons of the values of the dimensionless flow rate q_v^* and heat flux Φ^* exchanged at the cylinder exit obtained with and without TBLA.

Numerical results indicate that there is a difference between the local values of the fluid phase temperature and velocity, obtained with and without considering TBLA, only at the cylinder exit [Fig. 12(a) and (b)]. In fact, when the thermal boundary layer approximations are applicable, the second-order derivatives in the Z-direction of the temperature field will be negligible compared to those in the X-direction. Con-

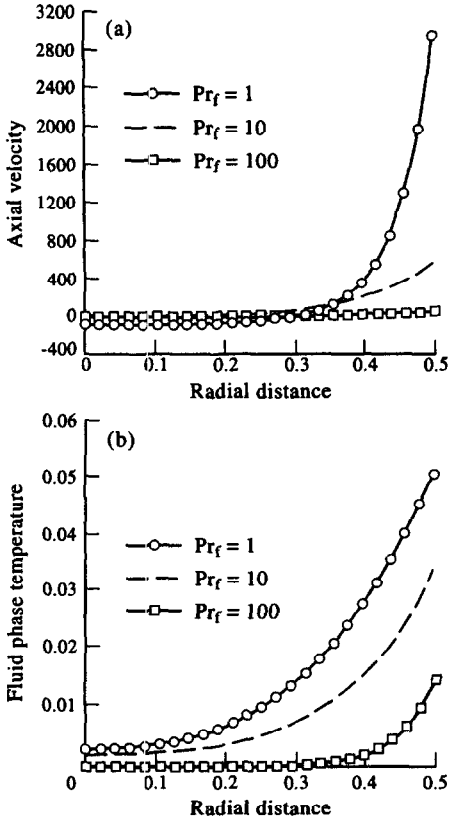

Fig. 11(a) Axial velocity vs radial distance at $Z = 0.5$; and (b) fluid phase temperature vs radial distance at $X = 0.5$ for $Gr_f = 10^8$, $A = 0.5$, $Da = 10^{-4}$, $\alpha_f/\alpha_s = 0.16$, $\Lambda_H = 0.057$, $Bi = 2 \times 10^3$ and for representative values of Prandtl number.

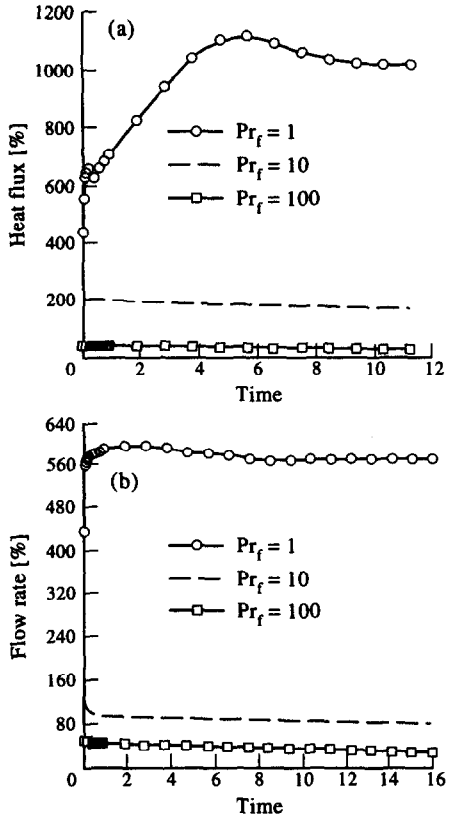

Fig. 13(a) Effects of the fluid Prandtl number, on the percent errors of the heat flux exchanged at the cylinder exit; and (b) of the flow rate obtained with and without TBLA, for $Gr_f = 10^8$, $A = 0.5$, $Da = 10^{-2}$, $\alpha_f/\alpha_s = 0.16$, $Bi = 2 \times 10^3$ and $\Lambda_H = 0.057$.

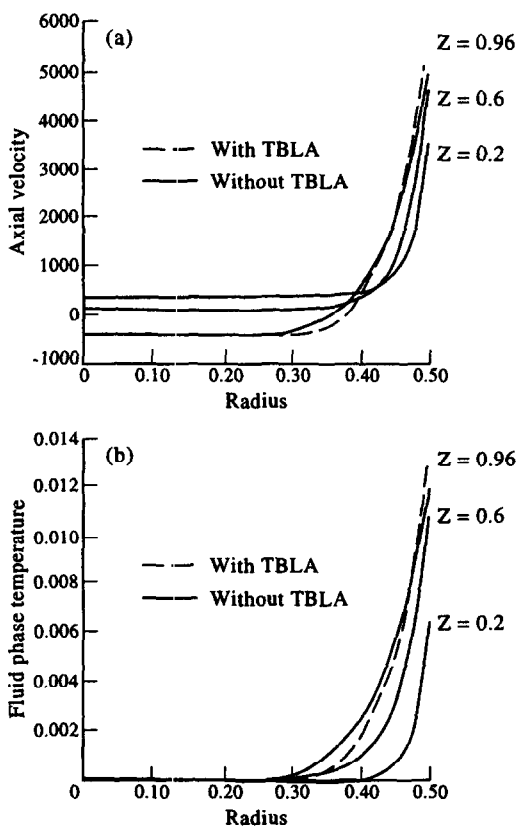

Fig. 12(a) Axial velocity vs radial distance obtained with and without TBLA; and (b) fluid phase temperature vs radial distance obtained with and without TBLA for $Gr_f = 5 \times 10^8$, $A = 0.5$, $Da = 10^{-4}$, $Pr_f = 10$, $\alpha_f/\alpha_s = 0.16$, $\Lambda_H = 0.057$, $Bi = 2 \times 10^3$ and at different axial locations.

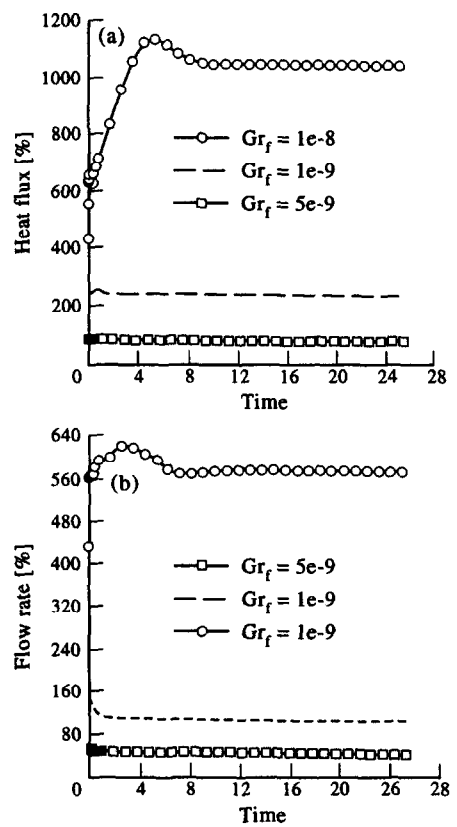

Fig. 14(a) Effects of the fluid Grashoff number, on the percent errors of the heat flux exchanged at the cylinder exit; and (b) of the flow rate obtained with and without TBLA, for $Pr_f = 0.71$, $A = 0.5$, $Da = 10^{-2}$, $\alpha_f/\alpha_s = 0.16$, $Bi = 2 \times 10^3$ and $\Lambda_H = 0.057$.

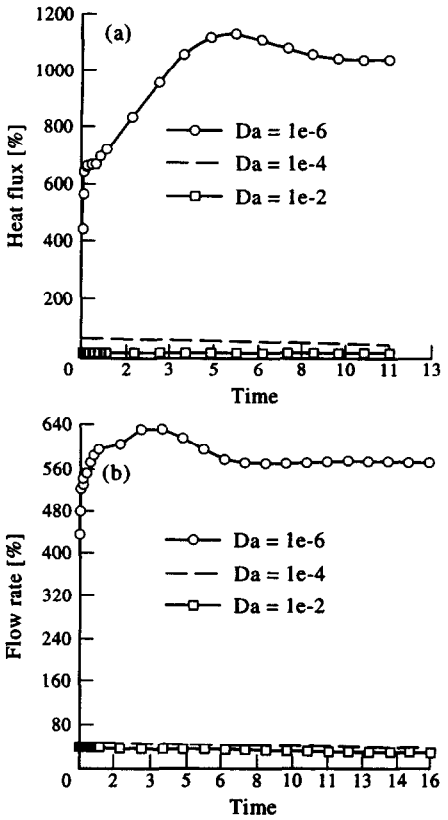

Fig. 15(a) Effects of the Biot number, on the percent errors of the heat flux exchanged at the cylinder exit; and (b) of the flow rate obtained with and without TBLA, for $Gr_f = 10^8$, $A = 0.5$, $Da = 10^{-2}$, $Pr_f = 0.71$, $\alpha_f/\alpha_s = 0.16$ and $\Lambda_H = 0.057$.

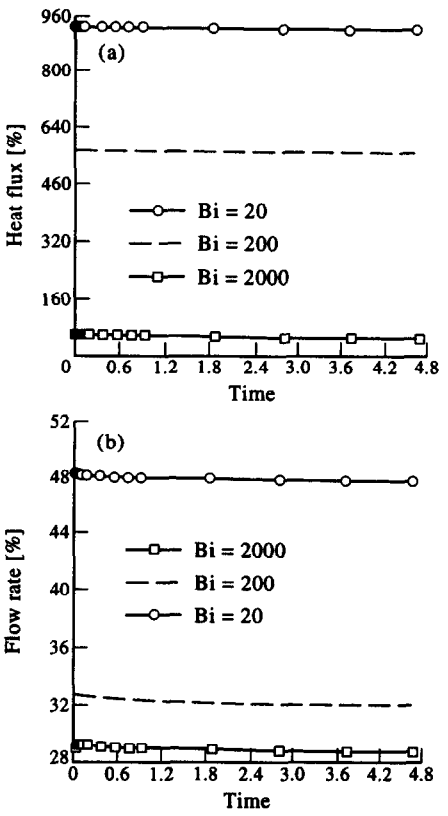

Fig. 16(a) Effects of the Darcy number, on the percent errors of the heat flux exchanged at the cylinder exit; and (b) of the flow rate obtained with and without TBLA, for $Gr_f = 10^8$, $A = 0.5$, $Bi = 2 \times 10^3$, $Pr_f = 0.71$, $\alpha_f/\alpha_s = 0.16$ and $\Lambda_H = 0.057$.

sequently, with TBLA, thermal boundary conditions at the cylinder exit are not considered. This will lead to an error in the numerical prediction of the temperature and the amount of heat that will be exchanged at the outlet face of the medium.

The relative differences between the values of q_∇^* and Φ^* obtained with and without TBLA increase when the Prandtl number Pr_f [Fig. 13(a) and (b)], the fluid Grashof number Gr_f [Fig. 14(a) and (b)], the Biot number Bi [Fig. 15(a) and (b)] and Darcy number Da [Fig. 16(a) and (b)] decrease.

4. CONCLUSION

Two-dimensional and transient fluid flow and heat transfer by natural convection in a vertical cylinder opened at both ends filled with a saturated porous medium and heated with a uniform lateral heat flux density was the focus of the present work. We have also studied the physical phenomena and the sensitivity to different parameters. Emphasis was also put on determining, in the considered conditions, the validity domains of the thermal boundary layer approximations (TBLA) and the Darcy flow model.

The numerical results show two types of flows (with and without top aspiration) which depend on the fluid Grashof number, the Darcy number, the fluid Prandtl number and the aspect ratio of the cylinder. Numerical findings also show that:

(1) In the considered conditions, there is a difference between the local values of the fluid temperature and velocity obtained with and without the use of thermal boundary-layer approximations only at the cylinder exit.

(2) The relative differences of the heat flux exchanged at the cylinder exit and the flow rate obtained with and without TBLA are high and increase when the fluid Prandtl number, Pr_f, the Grashof number, Gr_f, the Darcy number, Da, and the Biot number, Bi, decrease.

(3) If $Da \leqslant 10^{-4}$, the Darcy flow model is valid for all fluid Grashof number ranging from 10^8 to 5×10^9 and for all fluid Prandtl number ranging from 1 to 100.

REFERENCES

1. Bories, S., Natural convection in porous media. In *Advances in Transport in Porous Media*, eds J. Bear and M. Y. Corapcioglu. Martinus Nijhoff, Dordrecht, 1987.
2. Combarnous, M. and Bories, S., Hydrothermal convection in saturated porous media. *Advance in Hydrosciences*, 1975, **10**, 231–307.

3. Cheng, P., Heat transfer in geothermal systems. *Advances in Heat Transfer*, 1978, **14**, 1–105.
4. Nield, D. A., The stability of convective flows in porous media. In *Convection Heat and Mass Transfer in Porous Media*, Series E, Applied Sciences, Vol. 196. Kluwer Academic Publishers, Amsterdam, 1991.
5. Bejan, A. L., Natural convection in an infinite porous medium with a concentrated heat source. *Journal of Fluid Mechanics*, 1979, **89**, 97 and 107.
6. Hickox, C. E., Thermal convection at low Rayleigh number from concentrated source in porous media. *Journal of Heat Transfer*, 1981, **103**, 232–236.
7. Minkowycz, W. J. and Cheng, P., Free convection about a vertical cylinder embedded in a porous medium. *International Journal of Heat and Mass Transfer*, 1976, **19**, 205–813.
8. Larson, S. and Poulikakos, D., Double diffusion from a horizontal line source in an infinite porous medium. *International Journal of Heat and Mass Transfer*, 1986, **29**, 492–495.
9. Poulikakos, D., On buoyancy induced heat and mass transfer from a concentrated source in an infinite porous medium. *International Journal of Heat and Mass Transfer*, 1985, **28**, 621–629.
10. Cheng, P. and Minkowycz, W. J., Free convection about a vertical plate embedded in a porous medium with application to heat transfer from a dyke. *Journal of Geophysical Research*, 1977, **82**, 2040–2044.
11. Josh, Y. and Gebhart, B., Vertical natural convection flows in porous media: calculations of improved accuracy. *International Journal of Heat and Mass Transfer*, 1984, **27**, 69–75.
12. Bejan, A. and Poulikakos, D., The non Darcy regime for vertical boundary layer natural convection in porous medium. *International Journal of Heat and Mass Transfer*, 1984, **27**, 717–722.
13. Bejan, A. and Khair, K. R., Heat and mass transfer by natural convection in a porous medium. *International Journal of Heat and Mass Transfer*, 1985, **28**, 909–918.
14. Chamkha, A. J., Solar radiation assisted natural convection in uniform porous medium supported by a vertical flat plate. *ASME Journal of Heat Transfer* (in press).
15. Bejan, A., The boundary layer regime in a porous layer with uniform heat flux from the side. *International Journal of Heat and Mass Transfer*, 1983, **26**, 1339–1345.
16. Weber, J. E., The boundary layer regime for convection in vertical porous layer. *International Journal of Heat and Mass Transfer*, 1975, **18**, 569–573.
17. Masuouka, T., Yokote, Y. and Katsuhara, T., Heat transfer by natural convection in vertical porous layer. *Bulletin of JSME*, 1981, **24**, 995–1001.
18. Beukema, K. J. and Bruin, S., Three-dimensional natural convection in a confined porous medium with internal heat generation. *International Journal of Heat and Mass Transfer*, 1983, **26**, 451–458.
19. Ineba, H. and Sekin, N., A numerical study on transient heat transfer in a vertical porous layer. *Bulletin of JSME*, 1982, **25**, 934–938.
20. Lauriat, G. and Prasad, V., Natural convection in a vertical porous cavity: a numerical study for Brinkman-extended Darcy formulation in natural convection in porous media. *ASME*, 1987, **109**, 295.
21. Chang, W. J. and Hsiao, C. H., Natural convection in a vertical cylinder filled with anisotropic porous media. *International Journal of Heat and Mass Transfer*, 1993, **36**(13), 3361.
22. Combarnous, M. and Bories, S., Modélisation de la convection naturelle au sein d'une couche poreuse horizontale à l'aide d'un coefficient de transfert solide–fluide. *International Journal of Heat and Mass Transfer*, 1974, **17**, 505–515.
23. Bejan, A., Natural convection in vertical cylinder well filled with porous medium. *International Journal of Heat and Mass Transfer*, 1984, **23**, 726–729.
24. Thibaud, L., Contribution à l'étude de la convection naturelle à l'interieur d'un cylindre vertical poreux soumis à une densité de flux thermique pariétal constante. Thèse de l'Université de Poitiers, France, 1988.
25. Young, B. D., Williams, D. F. and Bryson, A. W., Two dimensional natural convection and conduction in packed bed containing a hot spot and its relevance to the transport of air in a coal dump. *International Journal of Heat and Mass Transfer*, 1986, **29**, 331–336.
26. Nishimura, T., Takumi, T., Shiraishi, M., Kawamura, Y. and Ozoe, H., Numerical analysis on natural convection in rectangular enclosure horizontally divided into fluid and porous region. *International Journal of Heat and Mass Transfer*, 1986, **29**, 889–898.
27. Ben Nasrallah, S., Amara, T. and Du Peuty, M. A., Convection naturelle instationnaire dans un cylindre rempli de grains ouvert à ses extrémités et dont la paroi est chauffée par un flux de chaleur constant-validité de l'hypothèse de l'équilibre thermique local. *International Journal of Heat and Mass Transfer*, 1997, **40**, 1115–1168.
28. Patankar, S. V., *Numerical Heat Transfer Fluid Flow*. Hemisphere/MacGraw-Hill, New York, 1980.
29. Vafai, K., Convective flow and heat transfer in variable porosity media. *Journal of Fluid Mechanics*, 1984, **147**, pp. 233–259.
30. Ward, J. C., Turbulent flow in porous media. *Journal of Hydraulics, Division of ASCE*, 1964, **90**, 1–12.
31. Ergun, S., Fluid flow through packed columns. *Chemical Engineering Progress*, 1952, **48**, 89–94.
32. Dullien, F. A. L., *Porous Media Fluid Transport and Pore Structure*. Academic, San Diego, CA, 1979.
33. Wakao, N., Kaguei, S. and Kunazkri, T., Effect of fluid dispersion coefficients on particle-to-fluid heat transfer coefficients in packed beds. *Chemical Engineering Science*, 1979, **34**, 325–336.
34. Hunt, M. L. and Tien, C. L., Non-Darcian convection in cylindrical packed beds. *ASME Journal of Heat Transfer*, 1988, **110**, 378–384.
35. Amiri, A. and Vafai, K., Analysis of dispersion effects and non-thermal equilibrium, non-Darcian, variable porosity incompressible flow through porous media. *International Journal of Heat and Mass Transfer*, 1994, **37**(6), 939–954.
36. Wakao, N. and Kaguei, S., *Heat and Mass Transfer in Packed Beds*. Gordon and Breach, New York, 1982.